The excited multiplet states of metalloporphyrins and metallophthalocyanines coordinated or linked to nitroxide radicals

2 AUTHORS, INCLUDING:

Nagao Kobayashi
Tohoku University

529 PUBLICATIONS   **11,512** CITATIONS

The excited multiplet states of metalloporphyrins and metallophthalocyanines coordinated or linked to nitroxide radicals

Kazuyuki Ishii, Nagao Kobayashi *

Department of Chemistry, Graduate School of Science, Tohoku University, Sendai 980-8578, Japan

Contents

Abstract

We have reviewed several time-resolved electron paramagnetic resonance (TREPR) studies focusing on influences of nitroxide radicals on the photophysical properties of metalloporphyrins and metallophthalocyanines, which are coordinated or linked to nitroxide radicals.

---

* Corresponding author. Fax: + 81-22-217-7719.

E-mail address: nagaok@mail.cc.tohoku.ac.jp (N. Kobayashi)

This paper summarizes TREPR studies on the excited multiplet states of metalloporphyrins and metallophthalocyanines coordinated by several kinds of nitroxide radicals, where the excited doublet and quartet states generated by the interaction between the excited triplet chromophore and doublet radical have been analyzed in detail. Selective population from the excited multiplet states to the triplet ground state is also discussed for phthalocyaninatosilicon covalently linked to two TEMPO radicals in terms of a new concept for controlling magnetic properties by photoexcitation. © 2000 Elsevier Science S.A. All rights reserved.

1. Introduction

Metalloporphyrins (MPs) and metallophthalocyanines (MPcs) coordinated or linked to nitroxide radicals (NRs) have been interestingly investigated by using time-resolved electron paramagnetic resonance (TREPR) spectroscopy [1–7]. TREPR is a useful method, by which many kinds of photoreaction intermediates, radicals and photoexcited triplet species, have been investigated [8–30]. Although photoexcited triplet species, which are diamagnetic in the ground state, have been intensively examined [8,9,31–37], there were few TREPR studies on photoexcited multiplet species, which are paramagnetic in the ground state [38–40]. If these excited multiplet states were observable, we would be able to obtain novel information such as electron spin polarizations (ESPs) and various EPR parameters, as in the case of the excited triplet states.

Recently, the first TREPR spectra of the excited doublet and quartet states have been observed for tetraphenylporphinatozinc(II) (ZnTPP) coordinated by p-pyridyl nitronyl nitroxide (p-nitpy), ZnTPP-p-nitpy, in the solid state (Fig. 1) [1,3]. These spectra were reasonably assigned and analyzed by using the g and zero-field splitting (zfs) parameter D values. The excited quartet EPR spectra with ESP were accurately simulated for the first time. The relationship between the ESP of the Q_1 state and spin-orbit coupling (SOC) was clarified for MPcs (M = Zn, Mg) coordi-
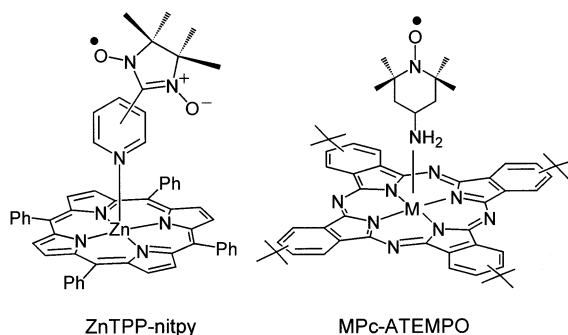

Fig. 1. Molecular structures of the ZnTPP-nitpy and MPc-ATEMPO (M = Zn, Mg) systems.

nated by 4-amino-2,2,6,6-tetramethyl-1-piperidinyloxy (ATEMPO) radical (Fig. 1) [7]. These results are important not only for establishing a method for evaluating the excited multiplet states, but also for investigating spin-sublevel dependence of quenching the excited singlet (S_1) and triplet (T_1) chromophores.

Recently, a novel phenomenon originating from the formation of the excited multiplet states has been observed for phthalocyaninatosilicon (SiPc) covalently linked to two TEMPO radicals, SiPc-(TEMPO)$_2$ (Fig. 2) [4]. The magnetic properties in the ground state after photoexcitation were investigated by TREPR measurements at room temperature, by which the photo-induced population transfer (PIPT) between the singlet ground (S_0) state and the triplet ground (T_0) state was observed [4]. This PIPT is attractive in terms of a new concept for controlling magnetic properties by photoexcitation.

In this paper, we review TREPR studies on the excited multiplet states of MPs and MPcs coordinated or linked to NRs. The ESPs of the excited quartet and doublet states in the solid state and the PIPT of SiPc-(TEMPO)$_2$ are illustrated.

2. The excited doublet and quartet states of ZnTPP and MPcs (M = Zn, Mg) coordinated by one nitroxide radical

2.1. Theoretical background

2.1.1. Wavefunctions of the excited doublet and quartet states

In the lowest excited singlet region, the $^1E_{ux}$ and $^1E_{uy}$ states are degenerate for ZnTPP and MPcs. The $^1E_{uy}$ ($^1E_{ux}$) state is constituted by two electronic configurations, $^1(a_{1u}e_{gx})$ and $^1(a_{2u}e_{gy})$ (or $^1(a_{1u}e_{gy})$ and $^1(a_{2u}e_{gx})$) [41–44]. In the case of ZnTPP, the a_{2u} and a_{1u} denote the highest occupied molecular orbital (HOMO) and 2nd HOMO, respectively. (In the case of MPcs, the a_{1u} and a_{2u} denote the HOMO and 2nd HOMO, respectively.) The e_{gx} and e_{gy} are the lowest unoccupied MOs (LUMO). Therefore, the wavefunctions of $^2(^1ZnTPP^*-^2NR)$ or $^2(^1MPc^*-^2NR)$, i.e. the D_3 and D_4 states, are expressed as follows [45–48].
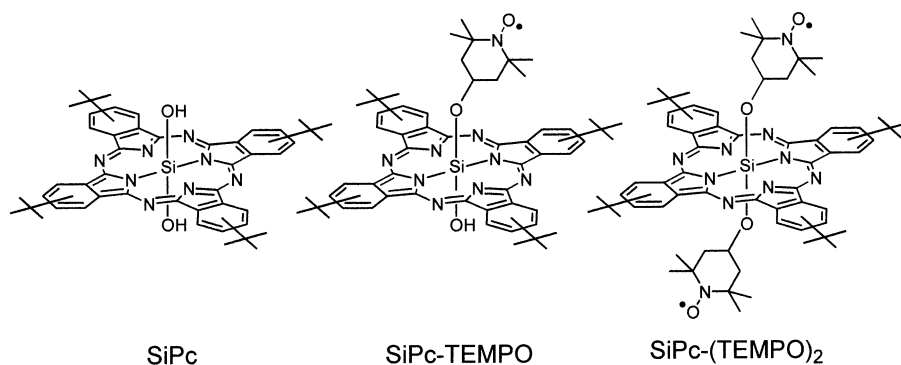

Fig. 2. Molecular structures of SiPc, SiPc-TEMPO, and SiPc-(TEMPO)$_2$.

$$|D_3, +1/2'> = \{\alpha(|a_{1u}\bar{e}_{gy}a_{2u}\bar{a}_{2u}r| - |\bar{a}_{1u}e_{gy}a_{2u}\bar{a}_{2u}r|)$$
$$- \beta(|a_{1u}\bar{a}_{1u}a_{2u}\bar{e}_{gx}r| - |a_{1u}\bar{a}_{1u}\bar{a}_{2u}e_{gx}r|)\}/\sqrt{2} \tag{1a}$$

$$|D_3, -1/2'> = \{\alpha(|a_{1u}\bar{e}_{gy}a_{2u}\bar{a}_{2u}\bar{r}| - |\bar{a}_{1u}e_{gy}a_{2u}\bar{a}_{2u}\bar{r}|)$$
$$- \beta(|a_{1u}\bar{a}_{1u}a_{2u}\bar{e}_{gx}\bar{r}| - |a_{1u}\bar{a}_{1u}\bar{a}_{2u}e_{gx}\bar{r}|)\}/\sqrt{2} \tag{1b}$$

$$|D_4, +1/2'> = \{\alpha(|a_{1u}\bar{e}_{gx}a_{2u}\bar{a}_{2u}r| - |\bar{a}_{1u}e_{gx}a_{2u}\bar{a}_{2u}r|)$$
$$- \beta(|a_{1u}\bar{a}_{1u}a_{2u}\bar{e}_{gy}r| - |a_{1u}\bar{a}_{1u}\bar{a}_{2u}e_{gy}r|)\}/\sqrt{2} \tag{1c}$$

$$|D_4, -1/2'> = \{\alpha(|a_{1u}\bar{e}_{gx}a_{2u}\bar{a}_{2u}\bar{r}| - |\bar{a}_{1u}e_{gx}a_{2u}\bar{a}_{2u}\bar{r}|)$$
$$- \beta(|a_{1u}\bar{a}_{1u}a_{2u}\bar{e}_{gy}\bar{r}| - |a_{1u}\bar{a}_{1u}\bar{a}_{2u}e_{gy}\bar{r}|)\}/\sqrt{2} \tag{1d}$$

Here, r denotes the singly occupied MO (SOMO) of NR. It is assumed that $\alpha = \beta = 1/\sqrt{2}$ for ZnTPP and that α and β of MPcs are equal to 1 and 0, respectively. On the other hand, the wavefunctions of $^2(^1\text{ZnTPP-}^2\text{NR*})$ or $^2(^1\text{MPc-}^2\text{NR*})$ are [45–48]

$$|D_n, +1/2'> = |a_{1u}\bar{a}_{1u}a_{2u}\bar{a}_{2u}d| \tag{2a}$$

$$|D_n, -1/2'> = |a_{1u}\bar{a}_{1u}a_{2u}\bar{a}_{2u}\bar{d}| \tag{2b}$$

Here, d denotes the highest doubly occupied MO or LUMO of NR.

In the lowest excited triplet region, the $^3E_{ux}$ and $^3E_{uy}$ states are degenerate, similarly to the $^1E_{ux}$ and $^1E_{uy}$ states. $^3\text{ZnTPP*}$ and $^3\text{MPc*}$ are known to be pure $^3(a_{2u}e_g)$ and $^3(a_{1u}e_g)$ configurations, respectively [37,49,50]. Therefore, the wavefunctions of $^{2,4}(^3\text{ZnTPP*-}^2\text{NR})$ are represented as follows [45–48].

$$|D_1, +1/2'> = (2|a_{1u}\bar{a}_{1u}a_{2u}e_{gx}\bar{r}| - |a_{1u}\bar{a}_{1u}a_{2u}\bar{e}_{gx}r| - |a_{1u}\bar{a}_{1u}\bar{a}_{2u}e_{gx}r|)/\sqrt{6} \tag{3a}$$

$$|D_1, -1/2'> = (-2|a_{1u}\bar{a}_{1u}\bar{a}_{2u}\bar{e}_{gx}r| + |a_{1u}\bar{a}_{1u}\bar{a}_{2u}e_{gx}\bar{r}| + |a_{1u}\bar{a}_{1u}a_{2u}\bar{e}_{gx}\bar{r}|)/\sqrt{6} \tag{3b}$$

$$|Q_1, +3/2'> = |a_{1u}\bar{a}_{1u}a_{2u}e_{gx}r| \tag{4a}$$

$$|Q_1, +1/2'> = (|a_{1u}\bar{a}_{1u}\bar{a}_{2u}e_{gx}r| + |a_{1u}\bar{a}_{1u}a_{2u}\bar{e}_{gx}r| + |a_{1u}\bar{a}_{1u}a_{2u}e_{gx}\bar{r}|)/\sqrt{3} \tag{4b}$$

$$|Q_1, -1/2'> = (|a_{1u}\bar{a}_{1u}a_{2u}\bar{e}_{gx}\bar{r}| + |a_{1u}\bar{a}_{1u}\bar{a}_{2u}e_{gx}\bar{r}| + |a_{1u}\bar{a}_{1u}\bar{a}_{2u}\bar{e}_{gx}r|)/\sqrt{3} \tag{4c}$$

$$|Q_1, -3/2'> = |a_{1u}\bar{a}_{1u}\bar{a}_{2u}\bar{e}_{gx}\bar{r}| \tag{4d}$$

The wavefunctions of the D_2 and Q_2 states are the same as Eqs. (3) and (4) with an exchange between the e_{gy} and e_{gx} orbitals. The wavefunctions of $^{2,4}(^3\text{MPc*-}^2\text{NR})$ are represented by Eqs. (3) and (4) with an exchange between the a_{1u} and a_{2u} orbitals.

2.1.2. EPR parameters

From the TREPR spectra of ZnTPP and MPcs coordinated by a nitroxide radical, EPR parameters, g and zfs parameter D values, can be obtained, and are confirmed by theoretical calculations. zfs matrix of the Q_1 state, $\boldsymbol{D}(Q_1)$, is represented as follows [51].

$$\boldsymbol{D}(Q_1) = \{\boldsymbol{D}(T_1) + \boldsymbol{D}(RT_1)\}/3 \tag{5}$$

Here, $D(T_1)$ and $D(RT_1)$ are zfs matrix for the excited triplet state and the magnetic dipole–dipole interaction between the excited triplet and the radical, respectively. For ZnTPP the matrix elements of the $D(RT_1)$, $D_{ij}(RT_1)$ $(i, j = x, y, z)$, were calculated under a point charge approximation as follows [37].

$$D_{ij}(RT_1) = (\mu_0 g^2 \beta^2/8\pi) \sum_s \sum_t (Cs_{a2u}^2 Ct_r^2 + Cs_{eg}^2 Ct_r^2)(r_{st}^2 \delta_{ij} - 3i_{st} j_{st})/r_{st}^5 \qquad (6)$$

$$r_{st}^2 = x_{st}^2 + y_{st}^2 + z_{st}^2$$

r_{st} is the distance between the s and t atoms. Cl_k denotes the k MO coefficient on the l atom. In the case of MPcs, $D(RT_1)$ was evaluated by exchanging between the a_{2u} and a_{1u} orbitals. In these calculations, the structures of ZnTPP and MPcs were determined with reference to the X-ray analyses. The MO coefficients of a_{2u}, a_{1u}, and e_g orbitals, calculated by the Pariser–Parr–Pople or ab initio method, were employed [52,53]. The coordination structure and SOMO of each nitroxide radical were calculated by using a PM3 hamiltonian [54]. The optimum structures were confirmed by comparison with the X-ray analyses [55–58]. In contrast, $D(T_1)$ was obtained from the TREPR measurement of ZnTPP or MPcs in the T_1 state. Using these $D(RT_1)$ and $D(T_1)$, the D value of the Q_1 state, $D(Q_1)$, was calculated by diagonalizing the $D(Q_1)$.

g values of the D_1 and Q_1 states, $g(D_1)$ and $g(Q_1)$, are expressed theoretically as follows [51].

$$g(D_1) = \{- g(R) + 4g(T_1)\}/3 \qquad (7)$$

$$g(Q_1) = \{g(R) + 2g(T_1)\}/3 \qquad (8)$$

The $g(R)$ value was estimated from the steady state EPR measurement of the doublet ground (D_0) state. The $g(T_1)$ was evaluated from the TREPR measurement of ZnTPP or MPcs in the T_1 state. $g(D_1)$ and $g(Q_1)$ were calculated using Eqs. (7) and (8), respectively.

2.1.3. Simulation method for excited quartet spectra

The excited quartet spectra were calculated using the following spin Hamiltonian, H_{spin}.

$$H_{spin} = g\beta BS + SDS = g\beta BS + D[S_z^2 - S(S+1)/3] + E(S_x^2 - S_y^2) \qquad (9)$$

Here, β is the Bohr magneton, S is the total electron-spin operator, g is the g tensor of electron spins, B is the external static magnetic field, D is the fine structure tensor, and D and E are the zfs parameters [3,59]. The resonance magnetic field ($B_{Ms \Leftrightarrow Ms+1}$) and transition probability ($TP_{Ms \Leftrightarrow Ms+1}$) for a single transition between Ms and Ms + 1 sublevels of the quartet state were calculated using the perturbation theory [59]. The calculated equations are applicable to these systems, since $v \sim 10$ GHz and $D < 0.3$ GHz.

In order to calculate the ESPs, eigenfunctions ($|Q,Ms>$; Ms = $-3/2$, $-1/2$, $1/2$, and $3/2$) at the resonance magnetic field are expressed by a linear combination of eigenfunctions at zero magnetic field, since the SOC between the excited doublet

state and excited quartet eigenfunctions at zero magnetic field is important for intersystem crossing (ISC). By diagonalizing a 4×4 matrix in Chart 1, the $|Q,Ms>$ is expressed by a linear combination of basis functions, $|Q,Ms'>$, which are eigenfunctions when $B_{Ms \Leftrightarrow Ms+1} = E = 0$, such as [3]

$$|Q,Ms> = \sum_{Ms'} C_{Ms,Ms'}|Q,Ms'> \tag{10}$$

Since the SOC between the excited doublet state and each $|Q,Ms'>$ is efficient for the ESP, the population of the $|Q,Ms>$ state, P_{Ms}, is represented by using the magnitude of SOC between the excited doublet and $|Q,Ms'>$ states, $P_{Ms'}$, as follows [3].

$$P_{Ms} = \sum_{Ms'} C^2_{Ms,Ms'} P_{Ms'} \tag{11}$$

Therefore, the ESP of a transition between the $|Q,Ms>$ and $|Q,Ms+1>$ sublevels, $P_{Ms \Leftrightarrow Ms+1}$, was calculated as

$$P_{Ms \Leftrightarrow Ms+1} = P_{Ms} - P_{Ms+1} \tag{12}$$

When the population of the upper sublevel, P_{Ms+1}, is larger than that of the lower sublevel, P_{Ms}, the $P_{Ms \Leftrightarrow Ms+1}$ is negative, and exhibits an emission of microwave. In contrast, when $P_{Ms+1} < P_{Ms}$, the $P_{Ms \Leftrightarrow Ms+1}$ is positive, and shows an absorption of microwave.

As a result, the line-shape function, $h(B)$, was calculated using $B_{Ms \Leftrightarrow Ms+1}$, $TP_{Ms \Leftrightarrow Ms+1}$, and $P_{Ms \Leftrightarrow Ms+1}$ as follows.

$$h(B) = \sum_{Ms} \int_0^{2\pi} d\varphi \int_0^{\pi} d\phi \int_0^{\pi/2} d\theta \, \sin\theta \, TP_{Ms \Leftrightarrow Ms+1} \times P_{Ms \Leftrightarrow Ms+1} \times f(B - B_{Ms \Leftrightarrow Ms+1}) \tag{13}$$

Here, $f(B - B_{Ms \Leftrightarrow Ms+1})$ is the line-shape function for a single transition, for which the Gaussian line-shape function was employed.

	$|Q,+3/2'>$	$|Q,+1/2'>$	$|Q,-1/2'>$	$|Q,-3/2'>$
$<Q,+3/2'|$	$D+(3/2)G_z$	$(\sqrt{3}/2)G_-$	$\sqrt{3}E$	0
$<Q,+1/2'|$	$(\sqrt{3}/2)G_+$	$-D+(1/2)G_z$	G_-	$\sqrt{3}E$
$<Q,-1/2'|$	$\sqrt{3}E$	G_+	$-D+(1/2)G_z$	$(\sqrt{3}/2)G_-$
$<Q,-3/2'|$	0	$\sqrt{3}E$	$(\sqrt{3}/2)G_+$	$D-(3/2)G_z$

$|Q,+3/2'> = |\alpha \, \alpha \, \alpha>$, $|Q,+1/2'> = \{|\alpha \, \alpha \, \beta> + |\alpha \, \beta \, \alpha> + |\beta \, \alpha \, \alpha>\}/\sqrt{3}$,

$|Q,-1/2'> = \{|\alpha \, \beta \, \beta> + |\beta \, \alpha \, \beta> + |\beta \, \beta \, \alpha>\}/\sqrt{3}$, $|Q,-3/2'> = |\beta \, \beta \, \beta>$

$G_z = g \, \beta \, B_{Ms \Leftrightarrow Ms+1} \cos\theta$, $G_{\pm} = g \, \beta \, B_{Ms \Leftrightarrow Ms+1} (\sin\theta \cos\phi \pm i\sin\theta \sin\phi)$

[a] D and E values are zero-field splitting parameters; θ and ϕ are the angle between the vector along the external magnetic field ($\vec{B}_{Ms \Leftrightarrow Ms+1}$) and the fine structure axis z and the angle between $\vec{B}_{Ms \Leftrightarrow Ms+1}$ and the fine structure axis x, respectively; $|Q, Ms'>$ (Ms=-3/2, -1/2, 1/2, and 3/2) are basis functions, which are eigenfunctions when $B_{Ms \Leftrightarrow Ms+1} = E = 0$.

(Chart 1)

2.2. Time-resolved EPR spectra of the excited doublet and quartet states

2.2.1. ZnTPP-nitpy systems

Absorption spectra of ZnTPP and p-nitpy in toluene are shown in Fig. 3. An absorption spectrum of m-nitpy is almost identical with that of p-nitpy. From the absorption spectrum, the lowest excited singlet state of ZnTPP is at 1.7×10^4 cm^{-1}. The lowest excited doublet state of p- or m-nitpy is estimated as 1.4×10^4 cm^{-1}. A phosphorescence spectrum of ZnTPP-p-nitpy at 77 K is also shown in Fig. 3. Since the phosphorescence maximum is detected at 793 nm, the energies of the D_1 and Q_1 states, ^{2,4}(^{3}ZnTPP*-^{2}nitpy), are estimated as 1.3×10^4 cm^{-1}. The energy diagram of the ZnTPP-nitpy system is shown in Fig. 4.

TREPR spectra of ZnTPP-p-nitpy and ZnTPP-m-nitpy observed at 20 K and 0.5 μs after laser excitation are shown in Fig. 5 together with a TREPR spectrum of ZnTPP coordinated by pyridine (ZnTPP-py). The TREPR spectra of the *para* and *meta* complexes are obviously different from that of ZnTPP-py, and indicate existence of interactions between ^{3}ZnTPP* and ^{2}nitpy. Two kinds of signals are observed for both ZnTPP-p-nitpy and ZnTPP-m-nitpy. One is relatively sharp signals with E ($g = 1.999 \pm 0.002$) and A ($g = 2.002 \pm 0.001$) polarizations for the *para* and *meta* complexes, respectively. Here, the A and E denote an absorption and
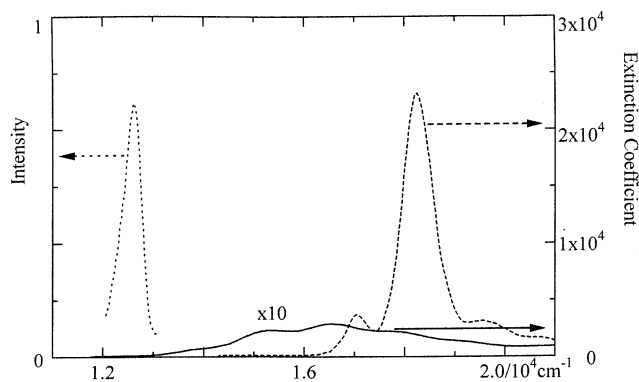

Fig. 3. Absorption spectra of ZnTPP (broken line) and p-nitpy (solid line) and a phosphorescence spectrum of ZnTPP-p-nitpy (dotted line). The absorption and phosphorescence spectra were observed in toluene at 293 and 77 K, respectively [3].
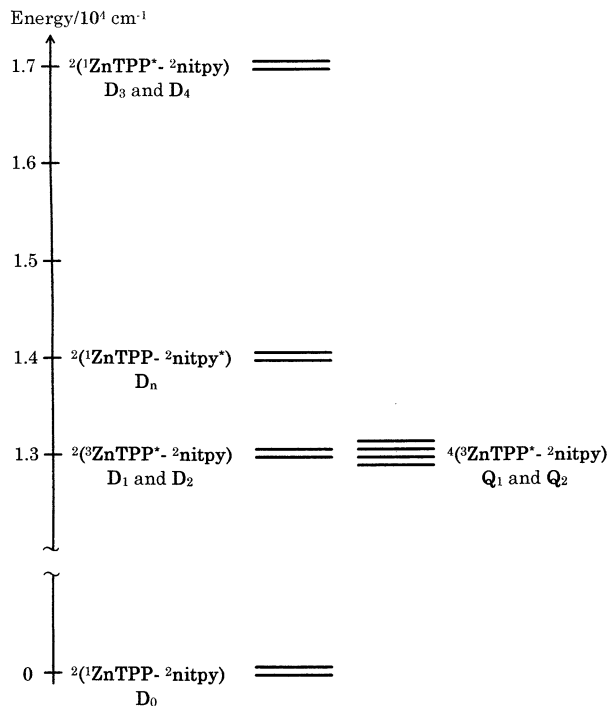
Energy/10^4 cm^{-1}

Fig. 4. An energy diagram of the ZnTPP-nitpy system. The D_3 and D_4 states are constituted by ZnTPP in the excited singlet state (^{1}ZnTPP*) and nitpy in the doublet ground state (^{2}nitpy). The D_n state originates from nitpy in the excited doublet state (^{2}nitpy*). The D_1, D_2, Q_1, and Q_2 states are generated by the interaction between ZnTPP in the excited triplet state (^{3}ZnTPP*) and ^{2}nitpy. The D_0 state denotes the doublet ground state.

an emission of the microwave, respectively. These sharp signals are assigned to the D_1 state, since the $g(D_1)$ values ($= 2.000$ and 2.001 for the *para* and *meta* complexes, respectively) calculated using $g(T_1) = 2.002$ are in good agreement with those observed. It has been proposed as an explanation of ESPs of the D_1 state that the internal conversion rate from the higher excited doublet states to $|D_1, +1/2>$ is different from that to $|D_1, -1/2>$ due to the contribution of the Q_1 state. The wavefunctions of the excited doublet state, $|D_1, I^\# >$, admixed with the Q_1 state due to the zfs interaction, H_{zfs}, are expressed as follows.

$$|D_1, I^\# > \; = N_I\{|D_1, I> \; + \sum_K (H_{I,K}/\Delta E_{I,K})|Q_1, K > \} \qquad (14a)$$

$$H_{I,K} = \; <Q_1, K|H_{zfs}|D_1, I > \qquad (14b)$$

$$\Delta E_{I,K} = 3J - \; <Q_1, K|H_{spin}|Q_1, K > \; + \; <D_1, I|H_{spin}|D_1, I > \qquad (14c)$$

The zfs interactions between the D_1 and Q_1 states for $B//z$ are shown in Fig. 6. When $J < 0$, the contribution of the Q_1 state to $|D_1, +1/2^\# >$ is larger than that to

$|D_1, -1/2^{\#}>$ due to the smaller energy difference. By this perturbation, the internal conversion rate to $|D_1, +1/2^{\#}>$ turns out to be slower than that to $|D_1, -1/2^{\#}>$. This difference results in the A polarization. In contrast, the internal conversion rate to $|D_1, +1/2^{\#}>$ is faster than that to $|D_1, -1/2^{\#}>$, when $J > 0$. This provides the E polarization. The observed E and A polarizations for the *para* and *meta* complexes are rationalized by using this proposed mechanism as well as J signs determined by TREPR experiments at room temperature, respectively [2].

The other is two pairs of signals giving an A/E polarization pattern. These A/E signals are reproduced very well by the excited quartet spectral simulations, as shown in Fig. 5. The spectral simulations indicate that the D value (0.22 GHz) of the *meta* complex is a little smaller than that (0.24 GHz) of the *para* complex, and that the populations of the $|Q_1, \pm 1/2'>$, $P_{\pm 1/2'}$, are larger than those of the $|Q_1, \pm 3/2'>$, $P_{\pm 3/2'}$, for both the *para* and *meta* complexes. Since $D(Q_1)$ values ($= 0.233$ and 0.224 GHz for the *para* and *meta* complexes, respectively) calculated using Eqs. (5) and (6) are almost the same as those evaluated by the spectral simulations, the A/E splittings are evidently assigned to the zfs in the Q_1 state. The
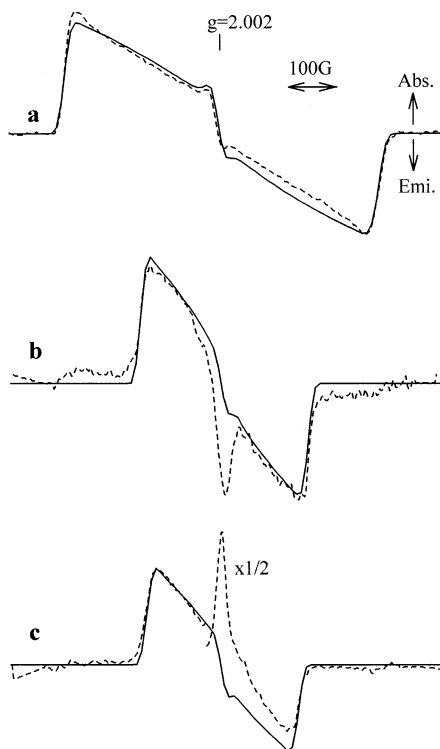

Fig. 5. TREPR spectra (broken lines) of ZnTPP-py (a), ZnTPP-*p*-nitpy (b) and ZnTPP-*m*-nitpy (c) with their simulations (solid lines; a–c). All spectra were observed at 20 K and 0.5 μs after laser excitation.
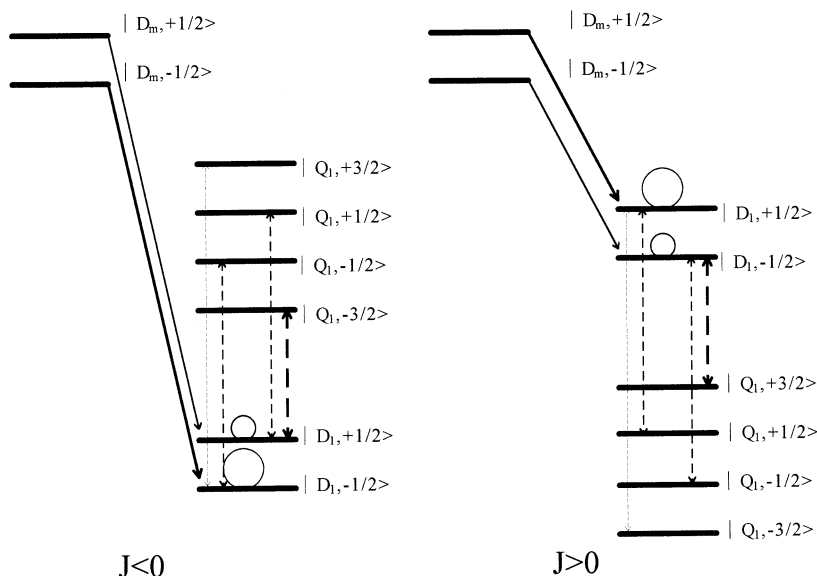
Fig. 6. Perturbation between the D_1 and Q_1 states. Arrows constituted by solid lines show internal conversion routes. Arrows constituted by broken lines represent the magnitude of the interaction between the D_1 and Q_1 states [3].

smaller $D(Q_1)$ of the *meta* complex originates from the negatively larger $D(RT_1)$. The selective ISC to $|Q_1, \pm 1/2'>$ spin sublevels is reasonably interpreted by SOC due to d_π atomic orbitals on the heavy zinc ion between the excited doublet and Q_1 states. The matrix elements of the SOC between the D_4 and Q_1 states and between the D_2 and Q_1 states were calculated using Eqs. (1), (3) and (4) as follows [37,45–48].

$$< D_4, I' | H_{SO} | Q_1, K' > \; = iZ/2\sqrt{3} \; (I = K) \tag{15a}$$

$$< D_4, I' | H_{SO} | Q_1, K' > \; = 0 \; (I \neq K) \tag{15b}$$

$$< D_2, I' | H_{SO} | Q_1, K' > \; = iZ/3\sqrt{2} \; (I = K) \tag{16a}$$

$$< D_2, I' | H_{SO} | Q_1, K' > \; = 0 \; (I \neq K) \tag{16b}$$

$$iZ = \eta^2 < d_{yz} | \xi \; l_z \; | d_{xz} >$$

Here, Z and η are a matrix element of SOC and the e_{gx} (e_{gy}) MO coefficient of the d_{xz} (d_{yz}) atomic orbital on the zinc ion, respectively. These calculation results, which indicate selective ISC to $|Q_1, \pm 1/2'>$, are consistent with the experimental results. On the other hand, the spin orbit interactions between the D_n and Q_1 states, between the D_3 and Q_1 states, and between the D_1 and Q_1 states can be ruled out by considering the MOs. Consequently, the selective ISC to $|Q_1, \pm 1/2'>$ is reasonably interpreted by the SOC between the D_4 and Q_1 states or between the D_2 and Q_1 states.
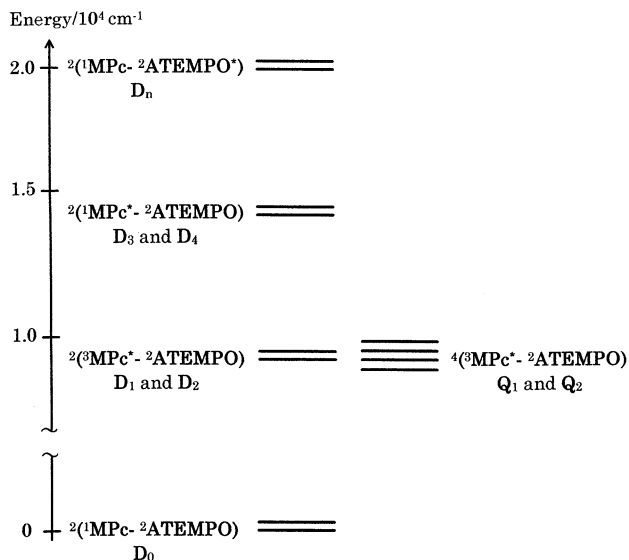
Energy/10^4 cm^{-1}

2.0 — $^2(^1MPc\text{-}\,^2ATEMPO^*)$ ══════
D_n

1.5 — $^2(^1MPc^*\text{-}\,^2ATEMPO)$ ══════
D_3 and D_4

1.0 — $^2(^3MPc^*\text{-}\,^2ATEMPO)$ ══════   ══════ $^4(^3MPc^*\text{-}\,^2ATEMPO)$
D_1 and D_2 Q_1 and Q_2

0 — $^2(^1MPc\text{-}\,^2ATEMPO)$ ══════
D_0

Fig. 7. An energy diagram of the MPc-ATEMPO system. The D_3 and D_4 states are constituted by ^{1}MPc* and ^{2}ATEMPO. The D_n state originates from ^{2}ATEMPO*. The D_1, D_2, Q_1, and Q_2 states are generated by the interaction between ^{3}MPc* and ^{2}ATEMPO. The D_0 state denotes the doublet ground state.

2.2.2. MPc-ATEMPO systems

With respect to the ISC to the Q_1 state, the component-dependence on SOC has been experimentally clarified in the MPc-ATEMPO (M = Zn and Mg) systems (Fig. 1) [7]. An energy diagram of MPc-ATEMPO is shown in Fig. 7 [19,60]. Since the energy of $^2(^1$MPc-^{2}ATEMPO*) is much higher than those of $^2(^1$MPc*-^{2}ATEMPO) and $^{2,4}(^3$MPc*-^{2}ATEMPO), the ISC to the Q_1 state can be investigated without taking into account $^2(^1$MPc-^{2}ATEMPO*). TREPR spectra of ZnPc-py and MgPc-py together with their simulations are shown in Fig. 8a and b, respectively. An A/E polarization pattern is observed for ZnPc-py, and is reproduced by selective ISC to a T_{1z} sublevel. This selectivity originates from the z component of SOC due to the d_π orbitals on the zinc ion [50,61]. On the other hand, the polarization pattern (E/A) of MgPc-py is reversed, and is reproduced by selective ISC to T_{1x} and T_{1y} sublevels. This selective ISC originates from the x and y components of SOC between π and σ (π^* and σ^*) orbitals, since the S_1 and T_1 states are admixed with ($\sigma\pi^*$) and ($\pi\sigma^*$) configurations via vibronic coupling [50,61]. The evaluated D values are 0.720 and 0.713 GHz for ZnPc-py and MgPc-py, respectively, and indicate the similarity of electronic structures between ZnPc-py and MgPc-py in the T_1 state. Therefore, the comparison between the Zn and Mg derivatives is evidently appropriate to extract effects of SOC, since only the components of SOC are varied without changing electronic structures.

TREPR spectra (broken lines) of ZnPc-ATEMPO and MgPc-ATEMPO are shown in Fig. 8c and d, respectively. Three signals are observed for both ZnPc-
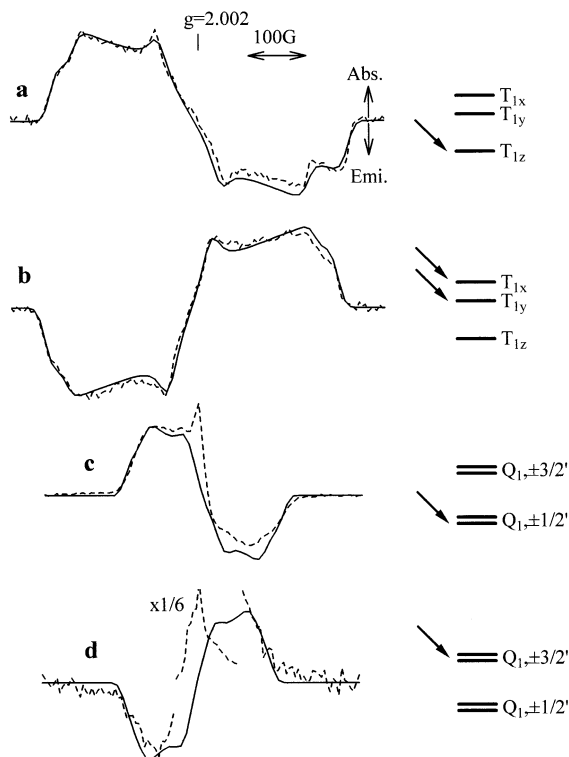
Fig. 8. TREPR spectra (broken lines) of ZnPc-py (a), MgPc-py (b), ZnPc-ATEMPO (c), and MgPc-ATEMPO (d) with their simulations (solid lines; a–d). These spectra were observed at 20 K and 0.7–1.3 μs after laser excitation [7].

ATEMPO and MgPc-ATEMPO. The polarization pattern of MgPc-ATEMPO is *EAA*, and is partially opposite to that (*AAE*) of ZnPc-ATEMPO. From the *g* values, the central *A* peaks are assigned to the D_0 and D_1 states for Zn and Mg complexes, respectively. On the other hand, the outer *E/A* signals for MgPc-ATEMPO and *A/E* signals for ZnPc-ATEMPO are simulated as the Q_1 states (Fig. 8c and d; solid lines). The TREPR spectrum of the Q_1 ZnPc-ATEMPO is reproduced using $D = 0.190$ GHz, $E = 0.035$ GHz, and $P_{+3/2'}:P_{+1/2'}:P_{-1/2'}:P_{-3/2'}$ $= 0:1:1:0$. On the other hand, the simulation spectrum of the Q_1 MgPc-ATEMPO is calculated using $D = 0.175$ GHz, $E = 0.035$ GHz, and $P_{+3/2'}:P_{+1/2'}:P_{-1/2'}:P_{-3/2'}$ $= 1:0:0:1$. Since the *D* values observed are similar to those ($= 0.16$ GHz) calculated under the point charge approximation, these outer signals are evidently assigned to the Q_1 state constituted by ^{3}MPc* and ^{2}TEMPO. The polarization pattern (*E/A*) of the Q_1 MgPc-ATEMPO is opposite to that (*A/E*) of the Q_1 ZnPc-ATEMPO. The spectral simulations indicate that the *A/E* and *E/A* polarization patterns originate from selective ISC to $|Q_1, \pm 1/2'>$ and to $|Q_1, \pm 3/2'>$, respectively. Consequently, it has been experimentally proved that ISC to $|Q_1, \pm 1/$

$2' >$ is selective due to the z component of SOC, while selective ISC to $|Q_1, \pm 3/2' >$ is promoted by the x and y components of SOC.

3. Phthalocyaninatosilicon covalently linked to one or two TEMPO radicals

3.1. Electronic absorption, MCD, and fluorescence spectra

UV-vis absorption, MCD, and fluorescence spectra of SiPc, SiPc-TEMPO, and SiPc-(TEMPO)$_2$ were observed at 293 K [6]. Absorption data of SiPc-TEMPO and SiPc-(TEMPO)$_2$ are very similar to those of SiPc, indicating that electronic interactions between the doublet TEMPO and the excited singlet SiPc are weak. The MCD data of SiPc-TEMPO and SiPc-(TEMPO)$_2$ are almost identical with those of SiPc, in analogy with the absorption spectra. This result can be reasonably explained by the fact that the MOs, which provide the orbital angular momentum, are localized on the Pc ring [62], and exhibit little interaction with the spin angular momentum of the TEMPO radicals.

In contrast, fluorescence quantum yield (Φ_F) values are remarkably dependent upon the number of TEMPO radicals. The Φ_F values of SiPc, SiPc-TEMPO, and
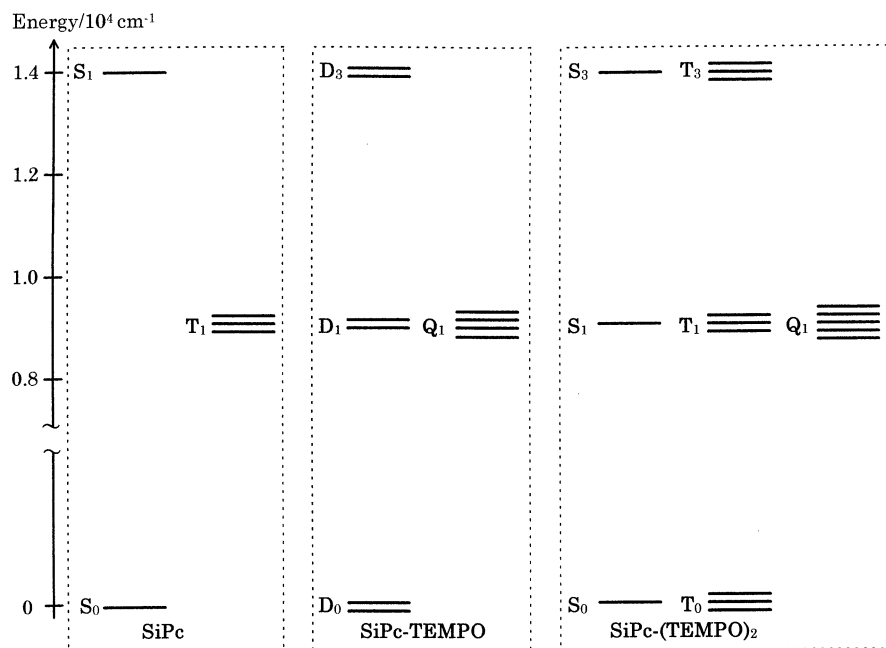

Fig. 9. Energy diagrams of SiPc, SiPc-TEMPO, and SiPc-(TEMPO)$_2$. The D$_3$ state of SiPc-TEMPO and the S$_3$ and T$_3$ states of SiPc-(TEMPO)$_2$ are constituted by the excited singlet SiPc and doublet TEMPO radicals. The D$_1$ and Q$_1$ states of SiPc-TEMPO and the S$_1$, T$_1$, and Q$_1$ states of SiPc-(TEMPO)$_2$ are constituted by the excited triplet SiPc and doublet TEMPO radicals.

SiPc-(TEMPO)$_2$ are 0.57, 0.21, and 0.012, respectively. The decrease in the Φ_F values is reasonably assigned to the change in ISC rate from ^{1}SiPc* to ^{3}SiPc*. The energy diagram of SiPc-TEMPO is different from that of SiPc, as shown in Fig. 9. For SiPc-TEMPO, the D$_3$ state is constituted by ^{1}SiPc* and ^{2}TEMPO. In contrast, the D$_1$ and Q$_1$ states are generated by the interaction between ^{3}SiPc* and ^{2}TEMPO. For SiPc the decay from ^{1}SiPc* to ^{3}SiPc* is spin-forbidden. However, the decay from ^{1}SiPc* to ^{3}SiPc* partially turns out to be a spin-allowed transition (D$_3 \rightarrow$ D$_1$) for SiPc-TEMPO. Therefore, the decrease in the Φ_F value of SiPc-TEMPO is rationalized by the formation of the D$_3 \rightarrow$ D$_1$ decay. The smallest Φ_F value of SiPc-(TEMPO)$_2$ is considered in a similar manner. The energy diagram of SiPc-(TEMPO)$_2$ is also shown in Fig. 9. The S$_3$ and T$_3$ states are constituted by ^{1}SiPc* and two ^{2}TEMPO radicals. Further, the S$_1$, T$_1$, and Q$_1$ states are generated by the interactions among ^{3}SiPc* and two ^{2}TEMPO radicals. Although nine spin sublevels are generated from ^{3}SiPc*, the spin quantum numbers of four sublevels are identical with that of the S$_3$ or the T$_3$ state. On the other hand, only two sublevels of the D$_1$ state out of six sublevels have the same spin quantum number as the D$_3$ state for SiPc-TEMPO. That is, the probabilities of spin-allowed sublevels are 1/3 and 4/9
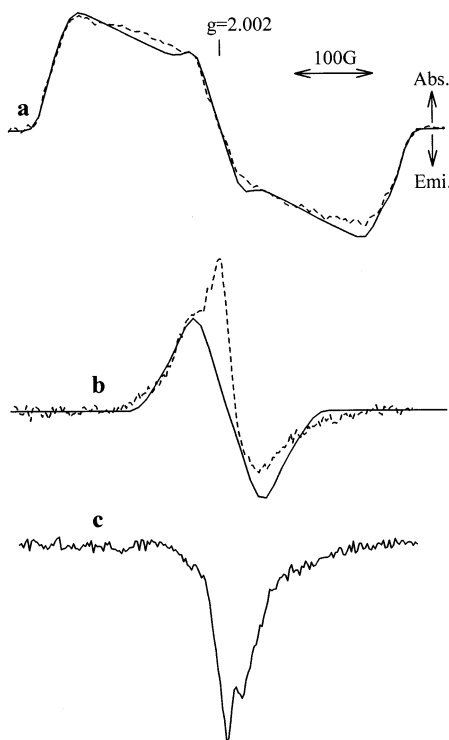

Fig. 10. TREPR spectra of SiPc (broken line; a), SiPc-TEMPO (broken line; b), and SiPc-(TEMPO)$_2$ (c) with their simulations (solid lines; a–b). These spectra were observed at 20 K and 0.6–0.9 µs after laser excitation.

for SiPc-TEMPO and SiPc-(TEMPO)$_2$, respectively. Therefore, the decay from ^{1}SiPc* to ^{3}SiPc* for SiPc-(TEMPO)$_2$ is faster than that for SiPc-TEMPO.

3.2. TREPR spectra in the solid state

TREPR spectra of SiPc, SiPc-TEMPO, and SiPc-(TEMPO)$_2$ were observed at 20 K, as shown in Fig. 10. An A/E polarization pattern is seen for SiPc, and is interpreted by selective ISC to T_{1z} sublevel. The D and E values of SiPc in the T_1 state are evaluated as 0.623 and 0.158 GHz, respectively. On the other hand, the TREPR spectrum of SiPc-TEMPO exhibits an AAE polarization pattern. The outer A/E signals of SiPc-TEMPO are simulated as the Q_1 state by using $D = 0.13$ and $E = 0.01$ GHz. Since the $D(Q_1)$ ($= 0.14$ GHz) calculated is almost the same as that evaluated by the spectral simulation, the outer A/E signals can be assigned to the Q_1 state constituted by ^{3}SiPc* and ^{2}TEMPO. The spectral simulation suggests that the selectivity of the ISC is $P_{+3/2'}:P_{+1/2'}:P_{-1/2'}:P_{-3/2'} = 0:1:1:0$, and can be interpreted by SOC between the P_x and P_y orbitals on the oxygen atoms of the
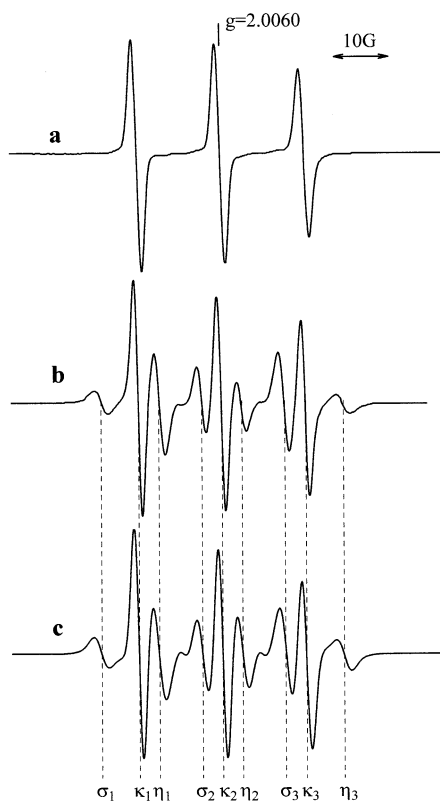

Fig. 11. Steady state EPR spectra of SiPc-TEMPO (a) and SiPc-(TEMPO)$_2$ (b). A simulation spectrum (c) was calculated as a spin-correlated radical pair by using $J = -5.3$ G.

axial-ligands. In contrast, the central A signal ($g = 2.007 \pm 0.002$) is assigned to the D_0 state by comparison with the steady state EPR spectrum, and the polarization is considered to be due to the excess β spin generated in the Q_1 state.

SiPc-(TEMPO)$_2$ shows an E signal in ca. 3290–3530 G region. Since the observed E signal is obviously different from that in the ground state, it is clearly assigned to the excited state. The S_1 and T_1 states decay fast to the S_0 and T_0 states, respectively, since they are spin-allowed internal conversion. On the other hand, the lifetime of the Q_1 state is long enough to be observable by the TREPR technique, since the decays from the Q_1 to the T_0 state and from the Q_1 to the S_0 state are spin-forbidden. Therefore, the E signal is considered to be attributed to the Q_1 state.
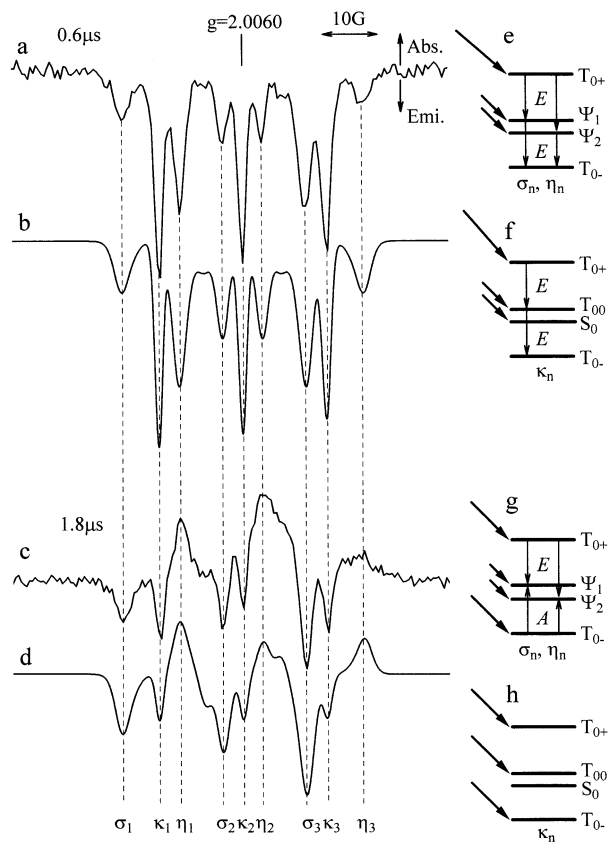

Fig. 12. TREPR spectra of SiPc-(TEMPO)$_2$ observed at 0.6 (a) and 1.8 μs (c) after laser excitation. Simulation spectra (b, d) were calculated by using parameters described in the text. Zeeman energy levels, selective populations from the excited multiplet states, and polarizations are shown for the signals of σ_n and η_n (e and g) and signals of κ_n (f and h), respectively. $|T_{0+}> (= |\alpha\alpha>)$, $|T_{00}> (= (|\alpha\beta> + |\beta\alpha>)/\sqrt{2})$, $|S_0> (= (|\alpha\beta> - |\beta\alpha>)/\sqrt{2})$, and $|T_{0-}> (= |\beta\beta>)$ denote the eigenfunctions of κ_n without the $S - T_0$ mixing. $|T_{0+}>$, $|\Psi_1> (= a|S_0> + b|T_{00}>)$, $|\Psi_2> (= -b|S_0> + a|T_{00}>)$, and $|T_{0-}>$ denote the eigenfunctions of σ_n or η_n with the $S-T_0$ mixing [4].

3.3. TREPR spectra in solution

Steady state EPR spectra of SiPc-TEMPO and SiPc-(TEMPO)$_2$, observed at 293 K, are shown in Fig. 11a and b, respectively. Three signals, split by hyperfine coupling of a nitrogen nucleus ($I = 1$), are observed for SiPc-TEMPO, indicating the presence of a TEMPO radical. On the other hand, SiPc-(TEMPO)$_2$ shows more complex EPR signals compared to the three signals of SiPc-TEMPO. Additional new signals are due to a spin-correlated radical pair constituted by two TEMPO radicals [16]. The observed spectrum was well simulated by using $J = -5.3$ G, as shown in Fig. 11c ($2J$ is the singlet–triplet splitting.).

TREPR spectra of SiPc-(TEMPO)$_2$ at 293 K, observed at 0.6 and 1.8 μs after laser excitation, are shown in Fig. 12a and c, respectively. By comparison with the steady state EPR spectrum (Fig. 11b), these signals are assigned to the spin-correlated radical pair in the ground state. The TREPR spectra at 0.6 and 1.8 μs show *EEE EEE EEE* and *EEA EEA EEA* polarization patterns, respectively. The signals of σ_n and η_n at 1.8 μs exhibit three pairs of *E/A* polarizations, which resemble the ESP of a spin-correlated radical pair generated from the triplet precursor, as observed for many kinds of photochemical reaction intermediates [14–17]. The TREPR spectrum at 0.6 μs is sufficiently reproduced by using $P(T_{0+}) = 0.5$, $P(T_{00}) = 0.25$, $P(S_0) = 0.25$, and $P(T_{0-}) = 0$, as shown in Fig. 12b. The *EEA EEA EEA* polarization pattern observed at 1.8 μs is reproduced by using $P(T_{0+}) = 0.46$, $P(T_{00}) = 0.24$, $P(S_0) = 0$, and $P(T_{0-}) = 0.3$, as shown in Fig. 12d. That is, the initial polarization is due to the excess α spin, and the later polarization originates from selective population to three triplet sublevels in the ground state.

The excess α spin at 0.6 μs in the ground state is assigned to the polarization generated in the excited state, since the TREPR spectrum at 20 K (Fig. 10c) indicates that the excess α spin is generated by selective ISC to the excited multiplet states. On the other hand, the later polarization is interpreted as follows. The decay from the Q_1 state to the T_0 state should be faster than that to the S_0 state, because the change in the spin quantum number between the Q_1 and T_0 states, $\Delta S = 1$, is smaller than that between the Q_1 and S_0 states, $\Delta S = 2$. Further, since the Q_1 state exists in the Boltzmann distribution after the spin-lattice relaxation, nearly equal population to three triplet sublevels in the ground state can occur. Therefore, the later *E/A* polarization is reasonably interpreted by selective decay from the Q_1 state in the Boltzmann distribution to three triplet sublevels in the ground state. In general, it is very difficult to change the difference in the population between the S_0 and T_0 states by varying the temperature, when $|2J| \sim 10^{-3}$ cm^{-1}, as with our biradical. Accordingly, it is noteworthy that the ground state generated via the excited multiplet states has more triplet character than that without photoexcitation, even at room temperature.

4. Conclusions

We have reviewed TREPR studies on the excited multiplet states of the paramagnetic complexes, ZnTPP-nitpy, MPc-ATEMPO, and SiPc-(TEMPO)$_n$. The TREPR

spectra of the excited doublet and quartet states can be reasonably assigned by using the g and D values. It is established that selective ISC, which is generated by SOC between the excited doublet states and eigenfunctions of the quartet state at zero magnetic field, determines the ESP of the excited quartet state. In contrast, the ESP of the D_1 state is interpreted by the difference between the internal conversion rate to $|D_1, +1/2>$ and that to $|D_1, -1/2>$. These results will motivate investigations of the other kinds of excited multiplet states, and become archetype in this field.

The photo-induced population transfer of SiPc-(TEMPO)$_2$ has been illustrated as an example of developments in the excited multiplet studies. It is different in principle from the previous mechanisms [63–70], where the magnetic properties are varied by changes in the electronic or chemical structures, to control the magnetic properties using the PIPT between the S_0 state and the T_0 state, where the electronic configuration is the same as that in the S_0 state. Therefore, this mechanism is not only attractive in terms of the physical chemistry but is also useful for controlling the magnetic properties in the ground state by photoexcitation. As an outlook, control of the macroscopic magnetism by photoexcitation should be attempted by building up polymers or crystals such as (-radical–chromophore-)$_n$ systems. Investigations of these possibilities will provide a novel approach to 'photo-controlled magnetism'.

Acknowledgements

References

[1] K. Ishii, J. Fujisawa, Y. Ohba, S. Yamauchi, J. Am. Chem. Soc. 118 (1996) 13079.
[2] J. Fujisawa, K. Ishii, Y. Ohba, S. Yamauchi, M. Fuhs, K. Möbius, J. Phys. Chem. A 101 (1997) 5869.
[3] K. Ishii, J. Fujisawa, A. Adachi, S. Yamauchi, N. Kobayashi, J. Am. Chem. Soc. 120 (1998) 3152.
[4] K. Ishii, Y. Hirose, N. Kobayashi, J. Am. Chem. Soc. 120 (1998) 10551.
[5] K. Ishii, Y. Hirose, N. Kobayashi, J. Phys. Chem. A 103 (1999) 1986.
[6] K. Ishii, Y. Hirose, N. Kobayashi, J. Porphyr. Phthalocyan. 103 (1999) 6060.
[7] K. Ishii, T. Ishizaki, N. Kobayashi, J. Phys. Chem. A 103 (1999) 6060.
[8] S.S. Kim, S.I. Weissman, J. Mag. Reson. 24 (1976) 167.
[9] S.S. Kim, S.I. Weissman, Rev. Chem. Intermed. 3 (1979) 107.
[10] S.K. Wong, D.A. Hutchinson, J.K.S. Wan, J. Chem. Phys. 58 (1973) 985.
[11] J.B. Pedersen, J.H. Freed, J. Chem. Phys. 62 (1975) 1706.
[12] F.J. Adrian, J. Chem. Phys. 54 (1971) 3918.

[13] F.J. Adrian, L. Monchick, J. Chem. Phys. 71 (1979) 2600.
[14] Y. Sakaguchi, H. Hayashi, H. Murai, Y.J. I'Haya, Chem. Phys. Lett. 110 (1984) 275.
[15] Y. Sakaguchi, H. Hayashi, H. Murai, Y.J. I'Haya, K. Mochida, Chem. Phys. Lett. 120 (1985) 401.
[16] C.D. Buckley, D.A. Hunter, P.J. Hore, K.A. McLauchlan, Chem. Phys. Lett. 135 (1987) 307.
[17] K. Tominaga, S. Yamauchi, N. Hirota, J. Chem. Phys. 92 (1990) 5175.
[18] C. Blättler, F. Jent, H. Paul, Chem. Phys. Lett. 166 (1990) 375.
[19] A. Kawai, T. Okutsu, K. Obi, J. Phys. Chem. 95 (1991) 9130.
[20] A. Kawai, K. Obi, J. Phys. Chem. 96 (1992) 52.
[21] A. Kawai, K. Obi, Res. Chem. Intermed. 19 (1993) 865.
[22] N.J. Turro, I.V. Khudyakov, S.H. Bossmann, D.W. Dwyer, J. Phys. Chem. 97 (1993) 1138.
[23] C. Corvaja, L. Franco, L. Pasimeni, A. Toffoletti, L. Montanari, Chem. Phys. Lett. 210 (1993) 355.
[24] C. Corvaja, L. Franco, A. Toffoletti, Appl. Magn. Reson. 7 (1994) 257.
[25] C. Corvaja, L. Franco, L. Pasimeni, A. Toffoletti, J. Chem. Soc. Faraday Trans. 90 (1994) 3267.
[26] M. Hugerat, A. van der Est, E. Ojadi, L. Biczok, H. Linschitz, H. Levanon, D. Stehlik, J. Phys. Chem. 100 (1996) 495.
[27] A. Regev, T. Galili, H. Levanon, J. Phys. Chem. 100 (1996) 18502.
[28] J. Fujisawa, K. Ishii, Y. Ohba, M. Iwaizumi, S. Yamauchi, J. Phys. Chem. 99 (1995) 17082.
[29] J. Fujisawa, Y. Ohba, S. Yamauchi, J. Phys. Chem. A 101 (1997) 434.
[30] W.S. Jenks, N.J. Turro, Res. Chem. Intermed. 13 (1990) 237.
[31] H. Murai, T. Imamura, K. Obi, Chem. Phys. Lett. 87 (1982) 295.
[32] H. Murai, T. Imamura, K. Obi, J. Phys. Chem. 86 (1982) 3279.
[33] M. Terazima, S. Yamauchi, N. Hirota, Chem. Phys. Lett. 98 (1983) 145.
[34] T.K. Chandrashekar, H. van Willigen, M.H. Ebersole, J. Phys. Chem. 88 (1984) 4326.
[35] O. Gonen, H. Levanon, J. Phys. Chem. 89 (1985) 1637.
[36] K. Ishii, S. Yamauchi, Y. Ohba, M. Iwaizumi, I. Uchiyama, N. Hirota, K. Maruyama, A. Osuka, J. Phys. Chem. 98 (1994) 9431.
[37] K. Ishii, Y. Ohba, M. Iwaizumi, S. Yamauchi, J. Phys. Chem. 100 (1996) 3839.
[38] G. Kothe, S.S. Kim, S.I. Weissman, Chem. Phys. Lett. 71 (1980) 445.
[39] C. Corvaja, M. Maggini, M. Prato, G. Scorrano, M. Venzin, J. Am. Chem. Soc. 117 (1995) 8857.
[40] C. Corvaja, M. Maggini, M. Ruzzi, G. Scorrano, A. Toffoletti, Appl. Magn. Reson. 12 (1997) 477.
[41] M. Gouterman, J. Chem. Phys. 30 (1959) 1139.
[42] M. Gouterman, J. Mol. Spectrosc. 6 (1961) 138.
[43] M. Gouterman, G.H. Wagniere, L.C. Snyder, J. Mol. Spectrosc. 11 (1963) 108.
[44] C. Weiss, H. Kobayashi, M. Gouterman, J. Mol. Spectrosc. 16 (1965) 415.
[45] D. Eastwood, M. Gouterman, J. Mol. Spectrosc. 30 (1969) 437.
[46] R.L. Ake, M. Gouterman, Theor. Chim. Acta 15 (1969) 20.
[47] M. Gouterman, R.A. Mathies, B.E. Smith, W.S. Caughey, J. Chem. Phys. 52 (1970) 3795.
[48] M. Gouterman, in: D. Dolphin (Ed.), The Porphyrins, vol. 3, Academic Press, New York, 1978, pp. 1–165.
[49] S.R. Langnoff, E.R. Davidson, M. Gouterman, W.R. Leenstra, A.L. Kwiram, J. Chem. Phys. 62 (1975) 169.
[50] K. Akiyama, S. Tero-Kubota, Y. Ikegami, Chem. Phys. Lett. 185 (1991) 65.
[51] A. Bencini, D. Gatteschi, EPR of Exchange Coupled Systems, Springer-Verlag, Berlin, 1990.
[52] N. Kobayashi, H. Konami, in: C.C. Leznoff, A.B.P. Lever (Eds.), Phthalocyanines — Properties and Applications, vol. 4, VCH, New York, 1996, pp. 343–404.
[53] H. Sekino, H. Kobayashi, J. Chem. Phys. 86 (1987) 5045.
[54] J.J.P. Stewart, J. Comp. Chem. 10 (1989) 209.
[55] D.M. Collins, J.L. Hoard, J. Am. Chem. Soc. 92 (1970) 3761.
[56] T. Kobayashi, T. Ashida, N. Uyeda, E. Suito, M. Kakudo, Bull. Chem. Soc. Jpn. 44 (1971) 2095.
[57] J.R. Mooney, C.K. Choy, K. Knox, M.E. Kenney, J. Am. Chem. Soc. 97 (1975) 3033.
[58] K. Awaga, T. Inabe, Y. Maruyama, Chem. Phys. Lett. 190 (1992) 349.
[59] Y. Teki, T. Takui, K. Itoh, J. Chem. Phys. 88 (1988) 6134.
[60] P.S. Vincett, E.M. Voigt, K.E. Rieckoff, J. Chem. Phys. 55 (1971) 4131.
[61] W.G. van Dorp, W.H. Schoemaker, M. Soma, J.H. van der Waals, Mol. Phys. 30 (1975) 1701.

[62] M.J. Stillman, T. Nyokong, in: C.C. Leznoff, A.B.P. Lever (Eds.), Phthalocyanines — Properties and Applications, vol. 1, VCH, New York, 1989, pp. 133–289.

[63] S. Decurtins, P. Gütlich, C.P. Köhler, H. Spiering, A. Hauser, Chem. Phys. Lett. 105 (1984) 1.

[64] S. Decurtins, P. Gütlich, K.M. Hasselbach, A. Hauser, H. Spiering, Inorg. Chem. 24 (1985) 2174.

[65] A. Hauser, Chem. Phys. Lett. 124 (1986) 543.

[66] P. Gütlich, A. Hauser, Coord. Chem. Rev. 97 (1990) 1.

[67] K. Itoh, Chem. Phys. Lett. 1 (1967) 235.

[68] E. Wasserman, R.W. Murray, W.A. Yager, A.M. Trozzolo, G. Smolinsky, J. Am. Chem. Soc. 89 (1967) 5076.

[69] Y. Teki, T. Takui, K. Itoh, H. Imamura, K. Kobayashi, J. Am. Chem. Soc. 108 (1986) 2147.

[70] O. Sato, T. Iyoda, A. Fujishima, K. Hashimoto, Science 272 (1996) 704.